

THE ILLINOIS CASCADE MICROTRON

A PROPOSAL FOR A HIGH DUTY FACTOR, INTERMEDIATE ENERGY ELECTRON ACCELERATOR

L. S. Cardman

Department of Physics and Nuclear Physics Laboratory  
University of Illinois at Urbana-Champaign  
Urbana, Illinois 61801

Summary

The Nuclear Physics Laboratory at the University of Illinois currently operates a 6-traversal Microtron Using a Superconducting Linac, MUSL-2, which provides 100% duty factor electron beams with energies between 2 and 80 MeV. We have submitted to the National Science Foundation a proposal to construct a 750 MeV cascade microtron capable of delivering 100% duty factor beams with currents of up to 100  $\mu$ A. Subharmonic RF splitting of the output beam will provide up to three simultaneous beams for experiments, with independently controllable currents (summing to 100  $\mu$ A). The proposal also includes two large building additions and the major new experimental equipment needed to exploit fully the research potential of this new accelerator.

Introduction

Our choice of 750 MeV as the design energy for our accelerator was based on a compromise<sup>1</sup> between the additional physics questions that can be addressed with higher energy beams and costs that escalate rapidly with energy. Continuous beams of 750 MeV electrons will permit the study of the nuclear response using both real and virtual photons over a range of excitation energies up to and including the delta resonance region. We are of the opinion that the beam energy must double, to 1.5 GeV, before many additional new nuclear phenomena become accessible to study. A research facility with a 750 MeV beam energy also provides an essential complement to the capabilities of the 4 GeV National Electron Accelerator Laboratory recommended by the Barnes Subcommittee<sup>2</sup> of NSAC.

The proposed accelerator consists of a linac injector followed by three cascaded racetrack microtron stages using room temperature radio-frequency (RF) linacs. This design provides an economical and reliable means for producing intermediate energy, high current, continuous electron beams. The microtron was chosen because of its well documented<sup>3,4,5</sup> cost-effectiveness for beam energies below 800 MeV. The cascade configuration is simple to construct and operate. In addition, our design can provide variable energy (80-180 MeV) parasitic beams for nuclear structure studies simultaneously with the higher energy beams from the third stage.

The major components of the Illinois Cascade Microtron are shown in Figure 1, and its principal characteristics are listed in Table 1. Three microtron stages are used in order to limit to 10 or less the ratio of the output energy to the input energy of each stage. This simplifies the optical design of the microtron and ensures excellent beam quality. The uniform field end magnets of the third microtron stage are large enough to bend 750 MeV electrons through a semicircle with a diameter of 3.51 meters. These end magnets can accommodate 90 orbits with an orbit spacing of 3.9 cm appropriate for a linac frequency of 2.45 GHz. The energy gain per traversal in the third stage is  $(750/90) \approx 8.33$  MeV. A very high quality 750 MeV beam can be obtained if the electrons injected into the third stage have an energy greater than 75 MeV. The second microtron stage is designed to provide electrons at seven discrete energies between 83.3 and 183.3 MeV with minimal changes in the

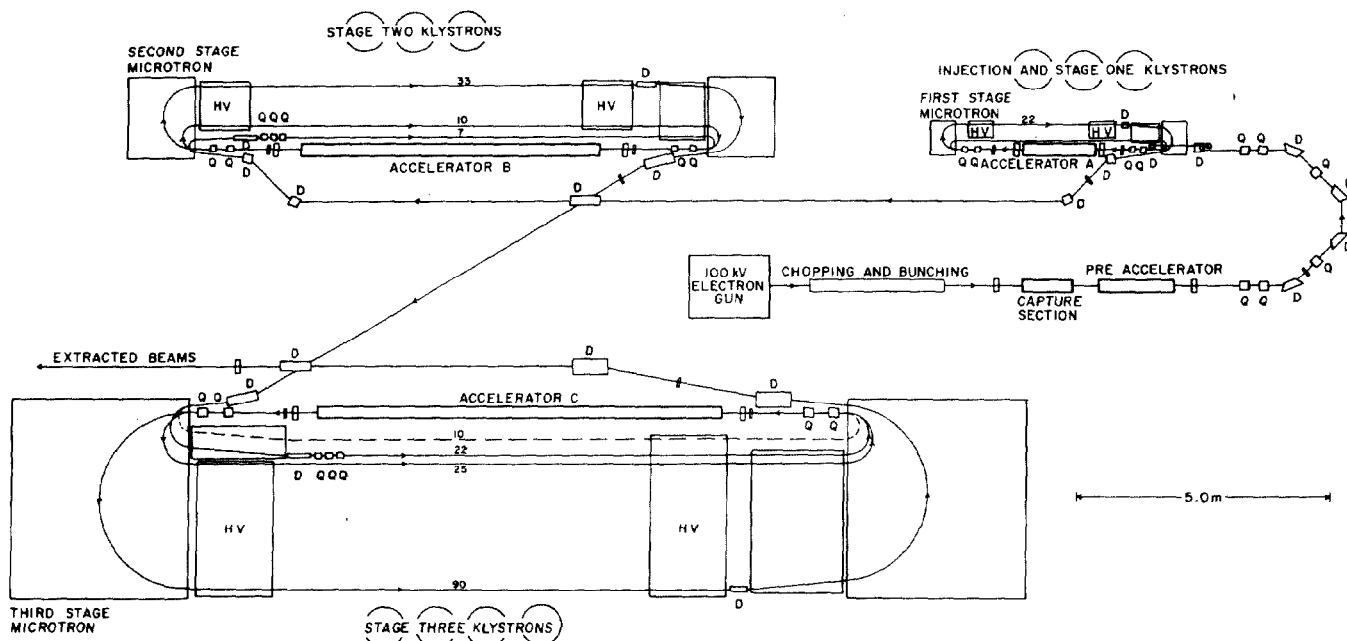


Figure 1 Plan view of the proposed Illinois Cascade Microtron

Table 1 Principal Characteristics of the Illinois Cascade Microtron

	Capture/ Pre-accelerator	Microtron Stage		
		1	2	3
Input Energy (MeV)	0.1	4.53	21.96	83.3 to 183.3
Output Energy (MeV)	4.53	21.96	83.3 to 183.3	750*
Number of Recirculations	----	17	11 to 29	60 to 68
Magnetic Field (tesla)	----	0.171	0.952	1.425
Outer Orbit Diameter (m)	----	0.86	1.29	3.51
Magnet Weight (each) (tons)	----	2	32	450
Accelerator Length (m)	5	1.0	5.9	8.8
Energy Gain per turn (MeV)*	4.43	1.015	5.355	8.333
Resonant Phase	----	20°	15°	15°
RF Power: Dissipated (kW)	81	17.78	84.11	126.10
Beam (kW)	0.45	1.74	6.13 to 16.13	66.7 to 56.7
Total (kW)	81.45	19.52	90.24 to 100.24	192.8 to 182.8

\*Lower energies available using fewer recirculations.

\*Energy gains listed are at the resonant phase. The energy gain per traversal varies significantly during the first traversals of the first stage microtron due to phase slip.

operating conditions of both the second and third stage microtrons. Other values of the interstage beam energy can be obtained by varying the energy gains and magnetic field values for both the second and the third microtron stages, maintaining the 2/3 ratio between the stages. A twenty percent variation in the operating parameters of the two stages is sufficient to provide an arbitrary interstage energy. The end magnets of the second stage microtron could accommodate 33 orbits; the 22 MeV injected beam will enter through the fourth return orbit. The 183.3 MeV output energy from the second stage would be achieved after 29 traversals through the 5.5 MeV linac; an 83.3 MeV output energy will be available after 11 traversals through this linac. The first microtron stage is the equivalent of a 22 orbit microtron with an energy gain per traversal of 1 MeV. A 4.5 MeV beam will be injected into this first stage; it will be extracted after 17 traversals of the linac.

Our microtron design benefits from components we have developed and experience we have gained in operating our present superconducting microtron, MUSL-2. We have also incorporated many of the subelements developed for room temperature microtrons at Mainz, NBS, Los Alamos, and Chalk River.

### General Design Considerations

The development of high duty cycle electron beams has been inhibited by the high capital and operating costs of conventional microwave linear accelerators. The problem can be understood<sup>4</sup> easily from the power equation for the linac design:

$$P_{rf} = \frac{DE^2}{RL} + P_{beam} \quad (1)$$

$P_{rf}$  is the time average RF power required,  $D$  is the macroscopic duty cycle,  $E$  is the energy gain,  $R$  is the shunt impedance per unit length,  $L$  is the length of the linac, and  $P_{beam}$  is the average beam power. Limitations on the average RF power per unit length of structure, and achievable shunt impedances had restricted single-pass linac designs to duty factors of a few percent. This limitation can be overcome by recirculating the beam many ( $N$ ) times through the same accelerating structure. In this case the power equation becomes

$$P_{rf} = \frac{D(E/N)^2}{R(L/N)} + P_{beam} = \frac{1}{N} \frac{DE^2}{RL} + P_{beam} \quad (2)$$

resulting in a substantial reduction in total power for a given beam power. The cascade microtron configuration is not as efficient as equation (2) would imply because of the power dissipated in the end magnets, the injector linac and earlier microtron stages. Nevertheless, the cascade microtron we propose requires only 5% of the RF power needed for a corresponding linac.

The resonance condition for the racetrack microtron with relativistic electrons is that the path length difference,  $\Delta L$ , between successive orbits should be an integral multiple,  $\nu$ , of the wavelength of the rf field, i.e.,  $\Delta L = \nu\lambda = \nu cT$ . For a uniform magnetic field,  $B$ , and a linac of energy gain  $\Delta E$  for electrons at the peak RF phase, the resonance condition can be expressed in terms of  $\phi_r$ , the resonant phase:

$$\frac{2\pi}{c} \Delta E \cos \phi_r = \nu\lambda B.$$

$\Delta E \cos \phi_r$  is the energy gain per recirculation. The

racetrack microtron is stable against phase variations if  $\phi_r$  is not too large:

$$0 < \phi_r < \tan^{-1} \left( \frac{2}{\pi\nu} \right).$$

The spacing,  $d$ , between successive recirculation orbits is:

$$d = \nu\lambda/\pi.$$

For a given radio frequency the orbit spacing increases with  $\nu$ , but the stable phase region decreases. We have chosen the  $\nu=1$  configuration for all three of our microtron stages because it provides the most efficient transformation of RF power into beam power.

The usefulness of the racetrack microtron configuration for high beam energies is limited by the stringent requirements ( $< 10^{-4}$ ) on field uniformity for the end magnets, which imply that  $B < 1.5$  tesla for conventional magnets. The linear dimensions of the end magnet are proportional to the desired beam energy,  $E$ . The weight of these magnets increases as  $E^3$ , and dominates the cost for energies greater than about 800 MeV.

Room temperature linacs were selected instead of superconducting linacs for our proposed accelerator to obtain substantially higher beam currents, to simplify construction, and to improve operational reliability. The threshold for recirculating beam breakup in our cascade microtron has been estimated using the theory of Lyness, et al.<sup>6</sup> to be over 500  $\mu A$ .

The optical design for all three of our microtron stages<sup>7</sup> is similar to the design of the Mainz microtrons<sup>7</sup> with all focussing elements on the common linac axis. The principal optical elements are the end magnets and quadrupole doublets placed at each end of the linac. The only optical elements planned for the recirculation paths are small vertical and horizontal steering coils at each end of each orbit. These steering coils are located in the rectangles marked HV in Figure 1 at each end of the recirculation system and can make small corrections to the individual orbits, thereby removing the effects of perturbations such as those caused by misalignments or small field errors in the end magnets. The end magnets will use the half picture frame design of Debenham,<sup>8</sup> and incorporate a Babic-Sedlacek<sup>9</sup> reverse field clamp to cancel the fringe field defocusing present in a conventional magnet. The quadrupole doublets are adjusted so that the first recirculation orbit has a betatron

oscillation phase shift of somewhat less than  $180^\circ$ . The increase in energy with each recirculation causes the betatron wavelength to grow with orbit number because the focal length of a quadrupole doublet increases as the square of the beam energy. This results in a beam size which is approximately constant throughout acceleration. This focusing arrangement is simple, and it locates the focusing elements along the common axis where there is no momentum dispersion in the beam. However, this weak focusing arrangement eventually allows the betatron oscillation wavelength to become too large, limiting the ratio of final to injected beam energies to a value of about 12. This effect can be seen in Figure 2, which displays the results of PTRACE<sup>10</sup> orbit calculations for the third microtron stage. It is this limit that results in our choice of the cascade configuration for our accelerator.

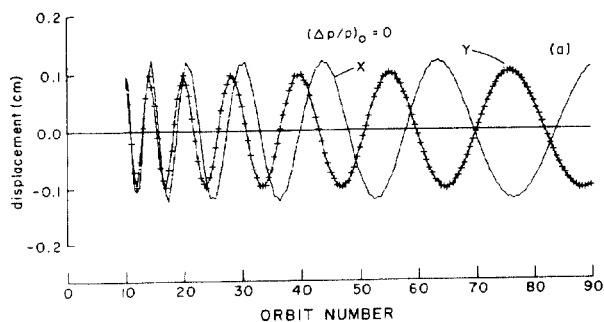


Figure 2 Calculated orbit trajectories for electrons injected 1 mm off axis into the third stage microtron

### Injector

The injector will provide a chopped, bunched beam with stable energy and small emittance, matched to the input requirements of the cascade microtron. In addition to cw operation, it will operate in a fast pulsed mode that will be used for tuneup diagnostics and that is desirable for some experiments. We will modify the injector being developed<sup>11</sup> for the NBS/LANL project to include subharmonic chopping.

The layout of the injector is shown in Figure 3. The electrons originate in a 100 kV, dc gun and associated pulser. The beam waist provided by the gun occurs at the center of the first lens,  $L_1$ , which focuses the beam on  $A_1$ , the first of two transverse emittance defining slits. The second transverse emittance defining slit,  $A_2$ , is located

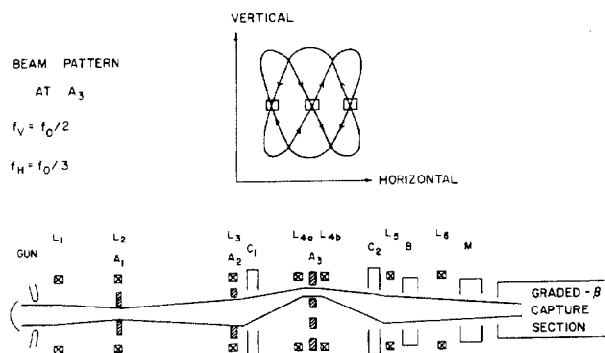


Figure 3 Plan view of the 100 keV injector beam line

0.5m downstream, just before the first chopping cavity,  $C_1$ . Chopping is performed by the system consisting of  $C_1$ ,  $L_{4A}$ ,  $A_3$ ,  $L_{4B}$ , and  $C_2$ .  $C_1$  is a chopping cavity which is excited at  $f_0/2$  in the vertical plane and  $f_0/3$  in the horizontal plane, where  $f_0$  is the resonant frequency of the microtron linacs. As a result, the beam pattern at the position of the chopping aperture is the Lissajou pattern shown in Figure 3. The chopping aperture will have slits with adjustable vertical openings at the positions of the crossovers in the horizontal plane (shown as small squares in Figure 3). The relative dimensions of these slits will define the relative beam currents for each of the three possible subharmonic beams by defining the sizes of the phase bunches sent to the buncher, capture section, and pre-accelerator. For full output current each slit will be adjusted to pass  $\pm 30^\circ$  phase bunches. The split lens  $L_{4A}$ ,  $L_{4B}$  images the

beam emerging from  $C_1$  at the second chopping cavity,  $C_2$ , which has its RF fields and their phases adjusted so that the transverse momentum given to the beam by  $C_1$  is exactly cancelled. The beam then passes through a bunching cavity, B, where a longitudinal accelerating field is applied to reduce the  $\pm 30^\circ$  phase bunch to  $\pm 5^\circ$  at the entrance of the capture section. The chopped, bunched beam is captured in a graded- $\beta$  linac structure with an average accelerating gradient of 1.5 MV/m. The captured, bunched beam is then sent to a preaccelerator consisting of two structures, one with  $\beta = 0.985$  and the second with  $\beta = 0.995$ , to achieve a 4.5 MeV final injector energy. The injector design can be expanded in the future to include the capability of delivering polarized electron beams. Both the 100 kV potential of the gun and the 100% duty cycle of the accelerator are well suited for polarized electron sources.

### First Microtron Stage

The beam from the injector linac will be dispersion matched to the input requirements of the first-stage microtron by the five magnet transport system shown in Figure 4. The field in the first dipole, D5, is set equal to the field in the microtron end magnet so that the beam emerging from D5 has exactly the transverse dispersion required for injection. This beam is then translated over the end magnet and back into the plane of the microtron by the four-magnet system  $D_{6a}$ ,  $D_{6b}$ ,  $D_{7a}$ , and  $D_{7b}$ , which is adjusted to be doubly achromatic. The beam enters the end magnet at the position of the fourth orbit, and emerges dispersion free on the linac axis after passing through the end magnet. Because the energy of the injected beam is high (4.53 MeV), the first recirculated beam easily clears the linac. This simplifies both the construction and operation of the microtron. The relatively high injection energy also increases the beam blowup threshold.

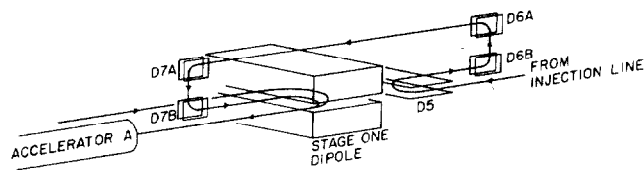


Figure 4 Detail of the injection trajectory into the first stage microtron

After the 4.53 MeV beam is injected into the microtron, seventeen recirculations raise the beam energy to 21.96 MeV. Extraction from the first microtron stage is effected by activation of a kicker dipole in the last recirculation orbit. This deflects the beam onto the extraction line for transport to the second stage.

### Second Microtron Stage

The second microtron stage has been designed, together with the injection scheme for the third microtron stage, to permit the development of parasitic electron beams in the intermediate energy range (from 80 to 180 MeV) for nuclear experiments by the addition of an rf beam splitter into the interstage transport.

The second stage end magnets are large enough to permit as many as 29 recirculations of the beam through a 5.55 MeV linac resulting in a maximum output energy of 183.3 MeV. Because the energy gain of the second stage linac is  $2/3$  the energy gain of the final stage linac, every third orbit in the second stage matches the energy of every second orbit in the third stage microtron. As a result, interstage beams can be obtained with energies in steps of 16.67 MeV with virtually no adjustment in the operating parameters of the two microtrons other than the positioning of the extraction kicker magnet on the recirculation orbit corresponding to the output energy desired from the second stage microtron and the positioning of the final injection dipole on the corresponding input orbit on the third stage microtron.

### Third Microtron Stage

The desired beam energy of 750 MeV governs the design of the third microtron stage. This energy, together with the magnetic field value, sets the scale for the end magnets which are a major component of the accelerator cost. The required pole dimensions are somewhat greater than  $1.75 \times 3.50$  meters for a field strength of 1.425 tesla in the end magnets. This field value has been chosen to ensure the high field uniformity ( $< 10^{-4}$ ) required for the end magnet. Input energies ranging from 83.3 to 183.3 MeV correspond to injection into the  $10^{\text{th}}$  through  $22^{\text{nd}}$  orbit.

The total number of orbits required to achieve the full 750 MeV output energy from the third stage microtron ranges from 80 to 68, depending on the injection energy. The flexibility associated with a range of interstage energies more than compensates for the modest increase in the complexity of the extraction and injection systems for the second and third stage respectively.

The extraction system, which is identical to the system employed on both the first and second stage microtrons, is shown in greater detail in Figure 5. For the extraction from the last ( $90^{\text{th}}$ ) orbit, the kicker magnet K3 is activated, sending the beam at a slight angle into the recirculation dipole. (The kicker provides a sufficient deflection to move the point at which the beam enters the end magnet by two orbit separations.) The displaced beam emerges at a complementary angle, easily clearing the elements on the linac axis, and enters the dipole D18 which forms the beginning of the transport to the experimental area. If a lower energy beam is desired, the kicker magnet is moved to a lower orbit. As an example, the trajectory for extraction from the  $64^{\text{th}}$  orbit (corresponding to a 533.3 MeV beam) is shown by the dashed lines on Figure 5. The kicker would be placed at the position K3' for this extraction energy.

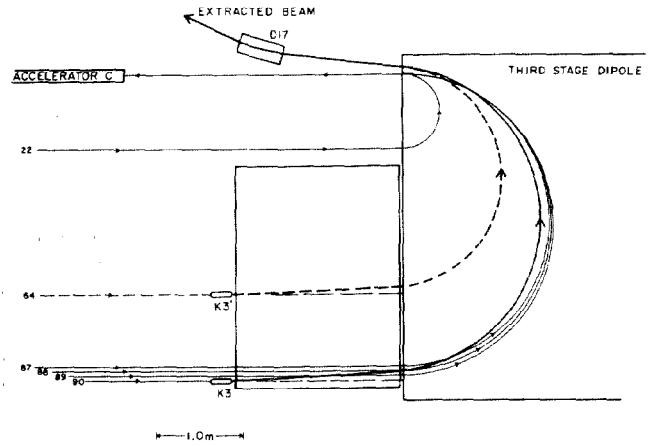


Figure 5 Detail of extraction trajectories from the third stage microtron

### Linac Structure and RF System

The linac structure we have included in our cascade microtron is the on-axis coupled design originally developed at Chalk River<sup>12</sup> and scaled by the Mainz group to 2.45 GHz. The Mainz group also modified this design by rotating the inter-cell coupling slots to reduce the sensitivity to recirculating beam blow-up<sup>13</sup>. Two 0.8 m lengths of this structure have been operating reliably in the Mainz first stage microtron, MAMI-1, since 1979. Two additional two meter lengths of this linac have recently been brought into operation at Mainz for the second stage microtron, MAMI-2. This structure has a shunt impedance of 67  $\text{M}\Omega/\text{m}$  and a coupling of 4%. When it is powered at a level of 15 kW/m, it produces an accelerating gradient of 1 MeV/m. A structure of this type is quite adequate for our cascade microtron. However, it may be possible to improve the performance of a linac with respect to capital costs, operating costs, and rf power requirements either by optimizing the on-axis design or by using an alternate cavity configuration.

We are currently collaborating with the Accelerator Physics group at the Chalk River Laboratory to investigate some of the factors that may lead to improvements in the existing cavity design. Tests are in progress on both the on-axis coupled structure and a co-axial coupled structure that could have a substantially greater resistance to beam blow up<sup>14</sup>. The beam cavity interaction will be studied<sup>15</sup> for both structures at the Chalk River Electron Test Accelerator (ETA). Full scale aluminum models of both structure designs have been fabricated and investigations of the coupling dependence on slot size and placement, and the mode and field distributions of both designs are in progress at Illinois. We are also studying ways of improving the power handling capability of the on-axis and coaxially coupled structures. The Mainz design has cooling channels only on the outer circumference of the structure. As a result, operation is normally restricted to a power level of 15 kW/m, corresponding to an accelerating gradient of 1 MV/m. Work done at Chalk River<sup>16</sup> on the effect of the addition of radial cooling channels which enter the web and nosecones of the 2.45 GHz, Mainz on-axis coupled structure indicates that it should be possible to run this structure at RF power levels of at least 35 kW/m. This would correspond to a

gradient of 1.5 MeV/m in a structure with a 67 MΩ/m shunt impedance. A theoretical model of the RF heating of the cavities and the corresponding dimensional changes that effect tuning has been developed, which provides good agreement with the frequency shifts measured at Mainz at 15 kW/m power levels.

We are also following closely the studies of the side-coupled structure in progress at LANL.<sup>17</sup> When these and our own studies have been completed, we will decide if any of these alternative designs are preferable to the proven Mainz design for our accelerator.

The RF system must be matched to the linac structure that is used in an accelerator. The Mainz version of the on-axis coupled structure has modest coupling (~4%). Because of this an rf power feed is required roughly every two meters. As the cascade microtron includes 20 meters of linac, approximately 10 rf power feeds are required. We have chosen to obtain this power using ten 50 kW cw klystrons (Thomson/CSF TH-2075), and to provide power level and phase control in the low level drive to the klystrons. Together with the GEM Group at ANL, we have developed a preliminary design for the power supply system for the Thompson klystrons. A single, large power supply will be used for two klystrons. Each klystron will be connected to the power supply through a series regulator which will provide 0.1% regulation and current limiting, and will also be capable of fast blocking under fault conditions. A single crowbar at the common high voltage will protect the power supply against catastrophic faults. The power supply, crowbar, and series regulators will be located in a separate building outside the accelerator vault and connected to the klystrons by high voltage cables. The klystrons themselves will be mounted in compact cabinets containing the filament and ion pump power supplies. They will be located in the accelerator cave adjacent to the linac sections they power to minimize the high power RF waveguide costs and the associated power losses.

#### Beam Diagnostics

The tuneup and operation of the cascade microtron will be simplified by incorporating beam diagnostic systems throughout the accelerator. These will include fluorescent viewscreen/TV monitors, wire scanners, and nonintercepting RF monitors. In addition, there will be beam loss monitors and radiation detection systems to simplify tuneup and to protect both the accelerator and personnel against component failure problems.

The fluorescent viewscreen monitors will be installed in all three microtron stages at each end of each linac and on the extraction paths to permit simple tuneup operations. They will also be used in the injector, on the extraction line, and in the interstage and experimental area transport.

Wire scanner beam monitors will be used to determine the transverse current profile of the accelerator beams. They will be included at the downstream end of each recirculation orbit to help adjust the steering coils needed to correct for small field errors in the end magnets. These wire scanners will be coupled mechanically so that a single measurement cycle will provide the profiles for all of the orbits at the same time. Additional wire scanners will be used in the injection line and the interstage transport lines. Each scanning wire will be equipped with a variable gain current-to-voltage converter to permit operation over a large dynamic range.

The most complex of the beam monitoring devices are the nonintercepting rf cavities. These can measure non-destructively the beam current, the RF phase, and the position of the beam centroid. For the version we plan to build, shown schematically in Figure 6, the beam will be passed through two cylindrical cavities. The first will provide information on beam displacements, while the second will provide intensity and phase information. These cavities will be made from aluminum, and will have very low Q values (~25); as a result they can be used with a fast pulsed beam to examine the behavior of all recirculating beams in the microtron.

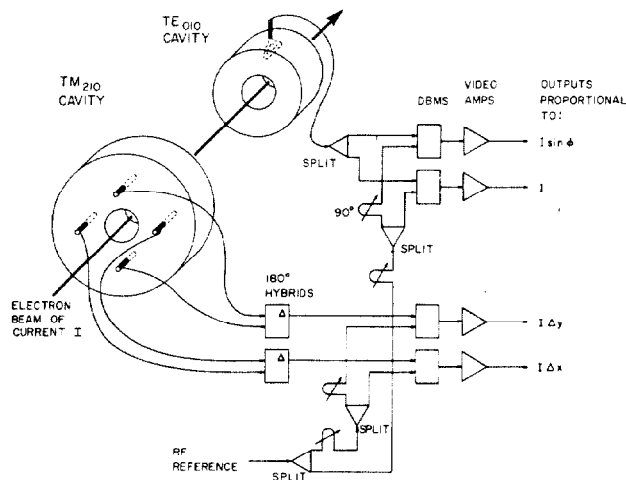


Figure 6 Schematic representation of a non-intercepting RF beam monitor

These RF monitors will be used in two applications. First, they will be placed on the injection line, on the two interstage transport lines, and on the exit beam line. The monitors at these locations will provide current and phase information about the beam as it passes between each major RF subsystem. The second set of RF monitors will be placed at each end of the linac in each microtron stage. These monitors will be most useful during the tuneup of the accelerator when the beam is in a pulsed mode. For pulse lengths shorter than the transit time of electrons for the shortest recirculation orbit, a low Q cavity placed on the axis of the microtron will see the beam as a series of excitations separated by the recirculation orbit times. It will be possible, therefore, to measure the current, phase, and displacement of each recirculating beam with a single cavity. The Mainz group<sup>18</sup> has used the information obtained in this manner to help the computer control system to optimize the tune of the MAMI-1 accelerator.

#### Computer Control System

The computer control system for the cascade microtron will consist of a distributed, multi-processor system with both autonomous and local network control of each station. The autonomous operation capability for each station will permit the use of computer control during the development phase of the accelerator for the testing and characterization of major subsystems. It will also allow the evolution of the control and monitoring software packages appropriate to the specific needs of that subsystem. The local network connection will provide access to all control and monitoring functions from a central station where system management functions ranging from the operator interface to record keeping can occur.

The distributed network we envisage, together with a more detailed drawing of a possible realization for a typical secondary station, is shown in Figure 7. The network consists of a total of five control secondaries linked to each other by a local area network bus. The network also links the secondaries to a primary control station. The secondary stations will be assembled using the MULTIBUS standard. A possible choice for the central microcomputer is the recently announced INTEL iAPX 432, a 32 bit processor having floating point capability and high computing power. The data acquisition and control interface will consist of two major parts. MULTIBUS interface boards will be used whenever commercially available modules provide a cost-effective solution to our needs. The remaining interfacing will use the Black Box interface standard, which was developed by the particle physics group at Illinois. This system provides a cost-effective, flexible, general purpose hardware standard for computer control. It is used extensively in the operation of MUSL-2 and its experimental areas, and a large inventory of modules and crates will be available for use with the new accelerator.

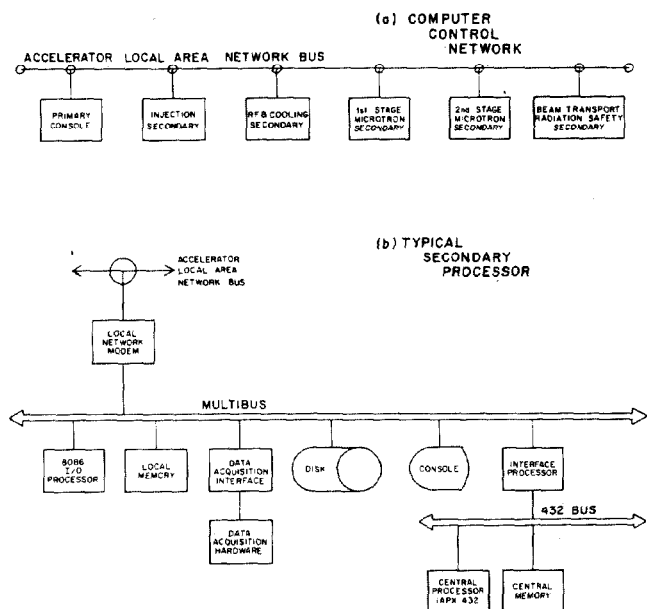


Figure 7 Computer Control Network

The primary console node will be similar to the secondary stations. However, a second iAPX 432 processor is provided for additional computing power, and an industry standard magnetic tape drive is provided for record keeping. Also provided are an expanded operator's console capable of controlling all accelerator elements, and connections to the laboratory computer network for interfacing experimenter demands and requests for information with the accelerator. The primary console node is linked to each of the secondary nodes by a local area network bus. We are evaluating both baseband (Ethernet) and broadband (CATV) networks to determine which will most effectively meet our needs.

#### Beam Transport to Experimental Areas

The transport system to the experimental areas begins with an energy analyzer, shown in Figure 8, which is a classical, 1.5m radius of curvature, DQD system<sup>19</sup> modified by the addition of quadrupole singlets before the first and after the second

dipole to permit variation of the focal properties. The pole face rotations and the quadrupoles will provide a spatial focus about 10 meters downstream that will be the secondary object for the remaining transport. Because the accelerator beam is expected to have an intrinsic energy spread of order  $10^{-4}$ , the energy analyzer will not be needed to define the energy spread of the beam delivered to the experimental areas. Instead, its function will be to stabilize long-term drifts in the microtron and to provide an absolute energy standard for the experimental beam. An RF subharmonic deflector operating at 816.67 MHz ( $1/3$  the linac frequency) can split the exit beam without any energy loss or beam loss. Such a device is shown downstream of the last energy analyzer element in Figure 8. The initial 2.45 GHz beam can be separated into either two or three beams by choosing the relative phase between the deflector and the linac RF systems. An alternate approach would be to incorporate about 1 MeV of 816.67 MHz accelerating linac between Q2 and D2 in the energy analyzer. This linac would introduce energy changes of the order of  $\pm 0.1\%$  into the bunches, rather than impart transverse momentum; separation would be effected by the action of the dipole D2 on these bunches. Because of the much higher efficiency of linac used in the accelerating mode, this scheme would require only about  $1/8$  of the RF power required by the transverse deflector.

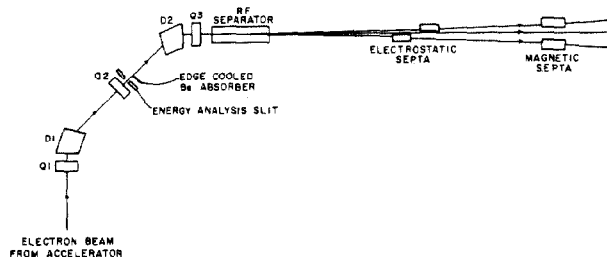


Figure 8 The energy analysis system and RF beam separator

For either RF separation technique, the beam centroids would be separated by about 1 cm a distance of 10 m downstream from D2. The separation would be completed by the addition of an electrostatic septum followed by a magnetic septum, as shown in Figure 8.

The remainder of the beam transport and the main features of our planned laboratory are shown on the site plan in Figure 9. The accelerator will be housed in an earth shielded vault near the south edge of our site. A new earth shielded experimental area, capable of accepting full intensity electron beams, will be constructed to house a 750 MeV/c electron spectrometer and an uncommitted beam line that can be used to test new experimental setups. The hall which presently houses MUSL-2 and two of its experimental areas will be renovated to house both a bremsstrahlung and a tagged photon facility. Two other possible beams are shown in Figure 9. Provision will be made to transport lower energy beams either to the existing 200 MeV/c electron spectrometer or to the existing Illinois low energy tagged photon facility. All of the major experimental areas will be shielded from each other so that each will be accessible whenever it is not in use.

### Acknowledgements

The operation of the Nuclear Physics Laboratory, and the development of this accelerator proposal were supported, in part, by the National Science Foundation under grant NSF PHY 80-23603. The proposal described in this article was the work of the entire Nuclear Physics Laboratory staff. Major contributions to the accelerator design were made by A. Hanson, R. Hoffswell, R. Laszewski, and A. Vetter. It is a pleasure to acknowledge invaluable contributions from our colleagues at Argonne, Chalk River, Los Alamos, Mainz, MIT-Bates, and Saclay.

### References

1. "Nuclear Physics Research with a 750 MeV Cascade Microtron", December, 1982 Report of the Nuclear Physics Laboratory, University of Illinois, Urbana, IL (unpublished).
2. "The Role of Electromagnetic Interactions in Nuclear Science", A Report of the DOE/NSF Nuclear Science Advisory Committee's Subcommittee on Electromagnetic Interactions, P. A. Barnes, chairman, Carnegie-Mellon University (1982).
3. J. S. Allen, *et al.*, *Particle Accelerators*, **1**, 239 (1970).
4. S. Penner, *IEEE Trans. Nucl. Sci.* **NS-28**, 2067 (1981).
5. H. Herminghaus, in "Proceedings of the Workshop on the Use of Electron Rings for Nuclear Physics Research in the Intermediate Energy Region", Lund, 1982 (to be published).
6. C. M. Lyneis, R. E. Rand, H. A. Schwettman, and A. M. Vetter, *Nucl. Inst. and Meth.* **204**, 269 (1983).
7. H. Aufhaus, *et al.*, p. 22 in "Proceedings of the 1981 Linear Accelerator Conference, Santa Fe, NM, Los Alamos National Laboratory Report LA-9234-C (1982).
8. P. H. Debenham, *IEEE Trans. Nucl. Sci.*, **NS-28**, 2885 (1981).
9. H. Babic' and M. Sedlacek, *Nucl. Inst. and Meth.* **56**, 170 (1967).
10. K. H. Kaiser, private communication.
11. M. A. Wilson, *et al.*, paper K-9, this conference.
12. S. O. Schriber, L. W. Funk, and R. M. Hutcheon, *Proc. 1976 Accelerator Conference, Atomic Energy of Canada, Ltd., Report AECL-5677*, p. 338 (1976).
13. H. Euteneuer, H. Herminghaus, and R. Klein, p. 239 in "Proceedings of the 1981 Linear Accelerator Conference", Santa Fe, NM, Los Alamos National Laboratory Report LA-9234-C, 22 (1982).
14. J.-P. Labrie and J. McKeown, *Nucl. Inst. and Meth.* **193**, 437 (1982).
15. K.C.D. Chan, H. Euteneuer, J.-P. Labrie, and J. McKeown, paper K-45, this conference.
16. J. McKeown and J.-P. Labrie, paper K-26, this conference.
17. L. M. Young and J. M. Potter, paper G-7, this conference.
18. H. J. Kreidel, p. 245 in "Proceedings of the 1981 Linear Accelerator Conference", *ibid.*
19. S. Penner, *Rev. Sci. Inst.* **32**, 150 (1961).

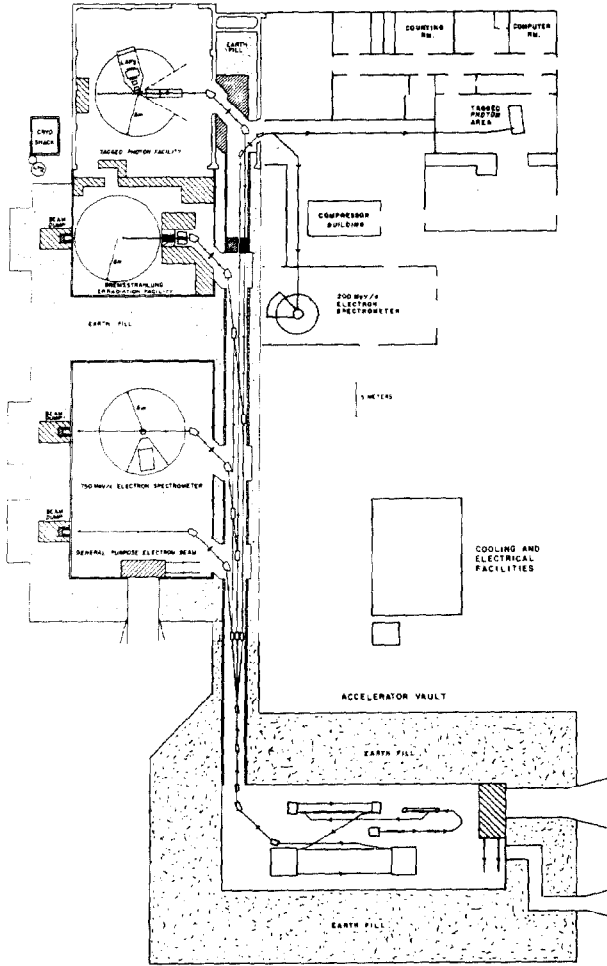


Figure 9 Site Plan for the proposed laboratory

Included in our proposal is major new experimental equipment designed to exploit fully the research potential of 750 MeV, 100  $\mu$ A, 100% duty factor beams. The magnetic spectrometers proposed include a 750 MeV/c electron spectrometer, a photon monochromator, and a charged pion spectrometer. The electron spectrometer will have a 35 msr solid angle,  $\pm 10\%$  momentum acceptance, and a momentum resolution better than  $5 \times 10^{-4}$ . The photon monochromator will have a  $\pm 40\%$  momentum acceptance and an intrinsic resolution of  $2 \times 10^{-4}$ . The charged pion spectrometer will have a 20 msr solid angle, a  $\pm 15\%$  momentum acceptance, and 0.5% momentum resolution. These spectrometers will be complemented by large scintillation arrays, photon and  $\pi^0$  detectors, and a variety of detectors for giant resonance decay products. The combination of this experimental equipment and high duty factor, intermediate energy electron beams can be expected to provide important new insights into the structure of atomic nuclei.